Coastal Dynamics 2017
Paper No. 143

SWASH DYNAMICS OF A SANDY BEACH WITH LOW TIDE TERRACE

Luis Pedro Almeida[1],Rafael Almar[2], Chris Blenkinsopp[3], Kevin Martins[4], Rachid Benshila[5] and Christopher Daly[6].

Abstract

A field experiment was conducted on a sandy beach with a low tide terrace (Nha Trang, Vietnam) to investigate the swash zone hydro- and morphodynamics throughout different tide and wave conditions. A 2D Lidar was used to measure runup properties and bed level changes on the swash zone. An energetic monsoon wave event provided energetic conditions during the initial stage of this experiment while mild wave conditions were observed during the remaining days. Swash dynamics were clearly modulated by wave and tide conditions. New insights on the intra-tidal swash morphodynamics were measured by the Lidar with individual tide cycles showing distinct phases of accretion and erosion. Tide was found to be the key factor underlying the interaction between surf and swash hydrodynamics and morphology.

Key words: Swash zone, wave runup, morphological changes, remote sensing.

1. Introduction

The swash is composed of two distinct phases, an upslope, landward directed, flow (uprush) and a downslope, seaward directed flow (backwash). Although there is a continuum of energy in swash spectra, they are commonly divided into incident (f > 0.05 Hz) and infragravity frequencies (f <0.05 Hz). The incident band is normally more energetic in bore-dominated, steeper intermediate and reflective beaches (Raubenheimer and Guza, 1996), while low sloped dissipative beaches have been observed to have most of the swash variance within infragravity frequencies (Ruggiero et al., 2004). Beaches with steep upper slope sand flat low-tide terraces (LTT) represent a special case where the three distinct hydrodynamic regimes (reflective, intermediate and dissipative) can be observed at different tide stages (Miles and Russell, 2004). Tide modulation of the wave breaking processes on the surf zone (e.g., plunging breakers at high tide breaking on the steeper section of the profile; spilling breakers during low tide breaking on the LTT), are expected to affect significantly the hydro- and morphodynamics of the swash zone of these environments, although with the exception of some studies on mixed sand and gravel beaches (e.g., Miles and Russell, 2004, or Kulkharni et al., 2006), these processes have not been investigated on sandy environments. The aim of the present work is to investigate the tidal effect on the inner-surf and swash hydro- and morphodynamics on a sandy, LTT beach using LIDAR observations. A 9-day field experiment was performed at Nha Trang beach (Vietnam), a microtidal sandy beach with a LTT. Variable wave and tide conditions were recorded and allowed an investigation of the link between tidal variations and inner-surf breaker characteristics, wave runup, swash asymmetry and morphological evolution.

[1]CNES/LEGOS, 18, av. Edouard Belin, 31401 Toulouse cédex 9, France. luis.pedro.almeida@legos.obs-mip.fr.
[2]IRD/LEGOS, 18, av. Edouard Belin, 31401 Toulouse cédex 9, France. rafael.almar@legos.obs-mip.fr.
[3]University of Bath, Claverton Down, Bath BA2 7AY, UK. c.blenkinsopp@bath.ac.uk.
[3]University of Bath, Claverton Down, Bath BA2 7AY, UK. k.martins@bath.ac.uk.
[4]University of Bath, Claverton Down, Bath BA2 7AY, UK. c.blenkinsopp@bath.ac.uk; k.martins@bath.ac.uk.
[5]Université de Bretagne Occidentale, Brest, France. christopher.daly@univ-brest.fr.

2. Methods

2.1 Study site

A field experiment was undertaken between 26 November and 4 December 2015 at Nha Trang beach, a sandy beach located on the South East of Vietnam (Figure 1). This medium-to-coarse sandy beach (D_{50} = 0.3 mm) has a fairly steep beach face slope (~ 0.1) and a narrow (~ 40 m) alongshore uniform and flat (~ 0.01) low tide terrace (LTT). The beach is a mixed wave-dominated micro-tidal environment (max tide range of 1.5 m), with a mix of diurnal and semi-diurnal tide. The wave climate in this area is strongly influenced by the two monsoon seasons, the northeast monsoon (NM) and the southwest monsoon (SM). The NM is characterized by strong winds (between 8-12 m/s), and energetic waves, occurring typically during the wet season (November to January), while the SM is characterized by mild wind and waves between June and September (Mau, 2014). In addition to the monsoon seasons, tropical cyclones, also known as Typhoons, can produce very energetic waves and surges in the region, resulting in infrequent but significant erosive events (Thuan et al., 2016).

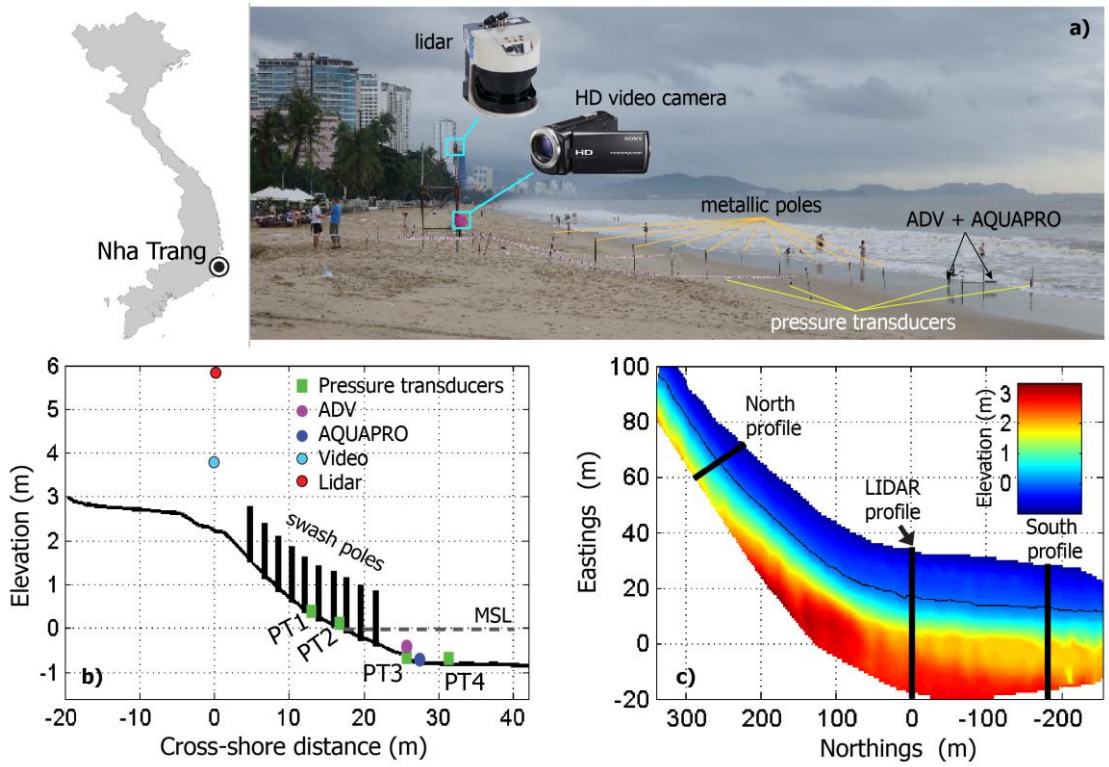

Figure 1. Geographical location of Nha Trang beach (dot on the top left map)Photo showing the instrumentation setup along a cross-section of the beach (a); beach profile with location of the instruments and indication of the mean sea level (MSL) during the present experiment (b); contour map of the study site topography with the location of the LIDAR profile and two additional profiles used in the present analysis (c).

2.2 Field observations

Swash zone hydrodynamics and morphological evolution were measured using one high frequency video camera HD (Sony HDR-CX 250) and 11 buried metallic poles painted in black (Figure 1). This method allows the collection of time series of high frequency (at 25 Hz) water surface elevation and bed level at each pole. A 2D Lidar (SICK LMS500) deployed on the top of a metallic tower (Figure 1) was used with the same propose, however providing an higher spatial resolution and range (distance between points of about 1 cm and maximum cross-shore range of about 30 meters each side of the scanner) than the swash video pole method. In addition to these two remote sensing instruments (video and Lidar), one scaffold rig

with one ADV (Nortek), one current profiler (Nortek - Aquapro) and one self-logging pressure transducer was installed on the inner part of the LTT, just at the intersection with the lower beach face (Figure 1). Three other self-logging pressure transducers were installed along the mid LTT, and on the mid and upper beach face (Figure 1). To complement these swash measurements an ADCP was moored offshore at 15 m depth to characterize the incoming offshore wave conditions (Figure 1). Daily topographic surveys were performed at every low tide (using RTK-GPS equipment) and covering 600 m to each side of the main instrument profile with a 10 m alongshore and 0.5 m cross-shore resolution. In the present work it was only used the ADCP, one pressure sensor, Lidar and beach survey datasets.

2.1.1. *2D Lidar*

The selected LIDAR for this work is a two-dimensional mid-range (maximum range ≈ 50 m) laser-scanner that emits pulsed laser beams (infrared light; λ = 905 nm) that are deflected on an internal mirror (inside the scanner head) that rotates at regular angular steps and scans the surroundings (180°) in a circular manner. The scanner head rotates at 25 Hz with an angular resolution of 0.166° and the distance to the target is calculated from the propagation time that the light requires from emission to reception of the reflection at the sensor. With this angular resolution and field of view, the instrument provided a spatial resolution that varied from 0.01 m at the Nadir point (zero grazing angle) to 0.4 m at the most seaward valid observation location (Figure 2). This spatial resolution allowed a complete coverage of the whole swash and inner-surf zone during the full duration of the experiment. The raw LIDAR measurements represent reflection of the laser beams from the beach topography as well as the water surface, without any distinction between the two (Figure 2b). To separate the topography from the water at each cross-shore position, and over time, a moving-average time window variance filter was applied to all measurements, following the approach described in Almeida et al. (2015). After initial data processing, the LIDAR measurements are separated in two distinct time series: (1) beach topography (Figure 2d) and (2) swash hydrodynamics (including water elevation and runup edge - Figure 2c). These time series form the basis of the analysis in the present work.

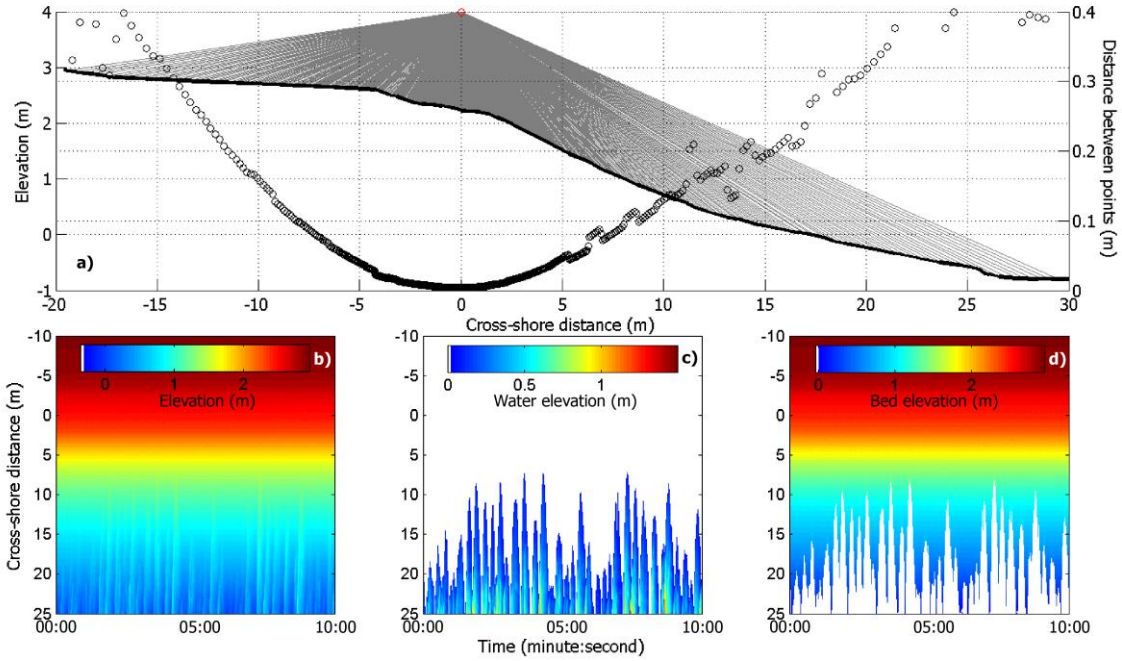

Figure 2. Beach profile with the indication of the LIDAR position and the theoretical projection of individual laser bea ms on the beach topography; the distance between observations (black dots) is computed as the horizontal distance bet ween consecutive laser beam measurements (a); the bottom panels show an example of raw LIDAR time-series (b) and post-process products: water elevation (c) and bed elevation (d) time-series.

3. Results

3.1. *Comparison between LIDAR and in-situ observations*

In order to assess the quality of the hydrodynamic (swash depth) and topographic (bed elevation) observations, a comparison between LIDAR and *in-situ* instruments (pressure sensor and RTK-GPS survey) was performed (Figure 3). The comparison between topographic observations performed by the LIDAR and RTK-GPS was performed using daily low-tide RTK-GPS topographic surveys performed precisely over the LIDAR scan transect. Results from this comparison (Figure 3a) show an excellent agreement (r^2 = 0.99 and *rmse* = 0.05 m) with differences within the magnitude of error of the RTK-GPS system (± 5 cm). Subsurface pressure observations from the pressure transducer number 3 (PT3) were converted to free surface elevation using linear theory and compared to direct free surface observations performed by the LIDAR (Figure 3b). The significant wave height computed as the 4σ, where σ is the standard deviation of the surface time series, for consecutive segments of 15 minutes of observations, was calculated for both instruments using time-synchronized time series measured at the location of the PT3 (Figure 2). Results show that observations performed with these two instruments correlate well (r^2 = 0.85 and *rmse* = 0.1 m), but the LIDAR consistently gives 30% larger estimates. A closer look into the two datasets (Figure 3c) allowed to identify that the cause of this difference is due to a consistent overestimation of the wave crest from the LIDAR. This higher LIDAR estimates of wave height may be owing to the presence of aerated wave roller or bore collapse, which would increase the elevation of the water surface measured by the LIDAR, while causing an underestimation of the pressure measured by the pressure transducer. This aspect illustrates an important advantage of the LIDAR, is that the high spatial resolution enables the instantaneous wave geometry to be captured rather than only time-series measurements at a small number of discrete points as discussed by Blenkinsopp et al. (2010) and Brodie et al. (2015).

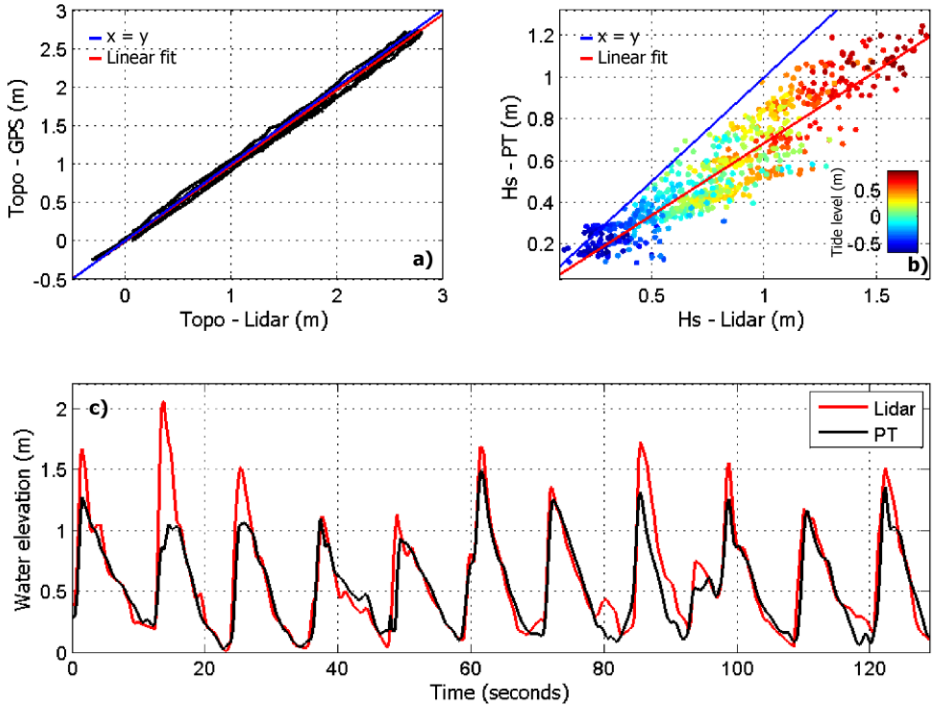

Figure 3. Scatter diagram of low-tide topographic surveys performed using RTK-GPS versus LIDAR topographic observations (a); scatter diagram of Hs computed from PT3 (see Figure 2) versus Hs computed from LIDAR, for the PT3 location; these comparisons were made using the entire datasets available (b); overlap of a time series of wave observations perform with the LIDAR (red line) and PT3 (black line) for 130 seconds of observations (c).

3.2. *Offshore wave conditions*

The wave and tide conditions during this experiment varied substantially (Figure 4a). The first days of the experiment (from the 27 until the 30 Nov 2015) were characterized by energetic swell (energetic single peak present in the wave spectra – Figure 4d) with offshore waves recorded by the moored ADCP showing Hs of between 0.9 and 1.3 m, and Tp between 8 and 12 seconds, during spring tides. The remaining four days of the experiment were characterized by mild wind waves, with offshore H_s under 1 m, Tp between 5 and 8 seconds and the tidal range gradually reducing to neap conditions (tidal range < 1 m). It is important to note that the mixed character of the tide (double high tide peak) was more pronounced during spring conditions and progressively become weaker under neap tides (Figure 4a).

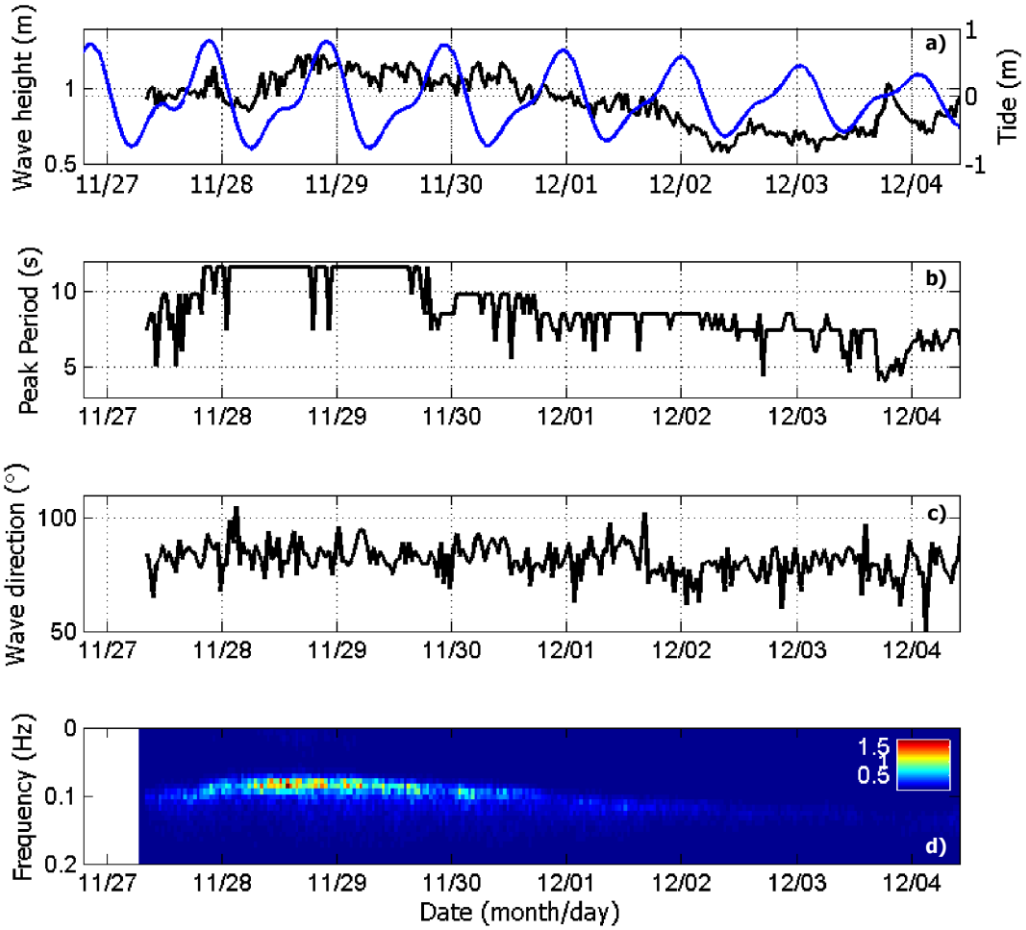

Figure 4. Tide (blue line) and offshore significant wave height wave measurements obtained from the ADCP (black line) moored at offshore location of the study site (a); wave peak period (b);mean wave direction (c); and bottom the normalized wave spectra as a function of time (d).

3.3. *Swash zone hydrodynamics*

Swash hydrodynamics of Nha Trang beach were investigated thought the calculation of the significant runup height (R_s) was computed as 4σ of the linearly detrended time series of shoreline elevation (R) within each 15 minute time window. The spectral signature of the R were analysed by computing the spectra for each time-window. Additionally, the Iribarren number (Battjes, 1974) for each window was computed based on the measured offshore wave characteristics and beach slope ($\xi = \beta / (H_s/L_0)^{1/2}$, where β is the swash slope observed by the LIDAR, and L_0 is the offshore wavelength).

Additionally, the front-to-lee horizontal runup asymmetry(A_s - hereinafter referred to as swash asymmetry) was computed as the third-order moment of the Hilbert transform (Kennedy et al., 2000):

$$A_s = \frac{\langle H^3(R_h - \overline{R_h})\rangle}{\langle (R_h - \overline{R_h})^2\rangle^{3/2}}$$

where H is the Hilbert transform and R_h the horizontal shoreline position. A_s includes the effect of energy dissipation due mainly to breaking and friction (Puleo & Holland, 2001) but also swash-swash interactions (Hughes & Mosseley, 2007) such as the catch-up and absorption of consecutive swashes during the uprush, and collision between uprush and preceding backwash. Negative A_s values are typically linked to swash events with asymmetric horizontal excursion where the uprush phase was much faster than the downrush. This type of swash event typically occur when two types of swash interaction are present: 1) two waves merging during the uprush phase, promoting enhanced uprush flow and downrush phase is only controlled by gravity; 2) downrush colliding with the following uprush, which promotes an important desacelaration of the downrush phase. Swash events with no interaction where found to have very low A_s values typically close to zero.
Time series of significant runup height (R_s) show a strong tidal modulation suggesting that tide is key factor controlling the swash hydrodynamics at Nha Trang beach. Wave power spectra calculations indicate that underlying the tidal modulation in the swash are distinct surf zone wave processes that occur at the different tide stages (Figure 5). Note that vertical runup power spectra were also computed but results showed a very similar signature to wave sprectrum and are not presented here.

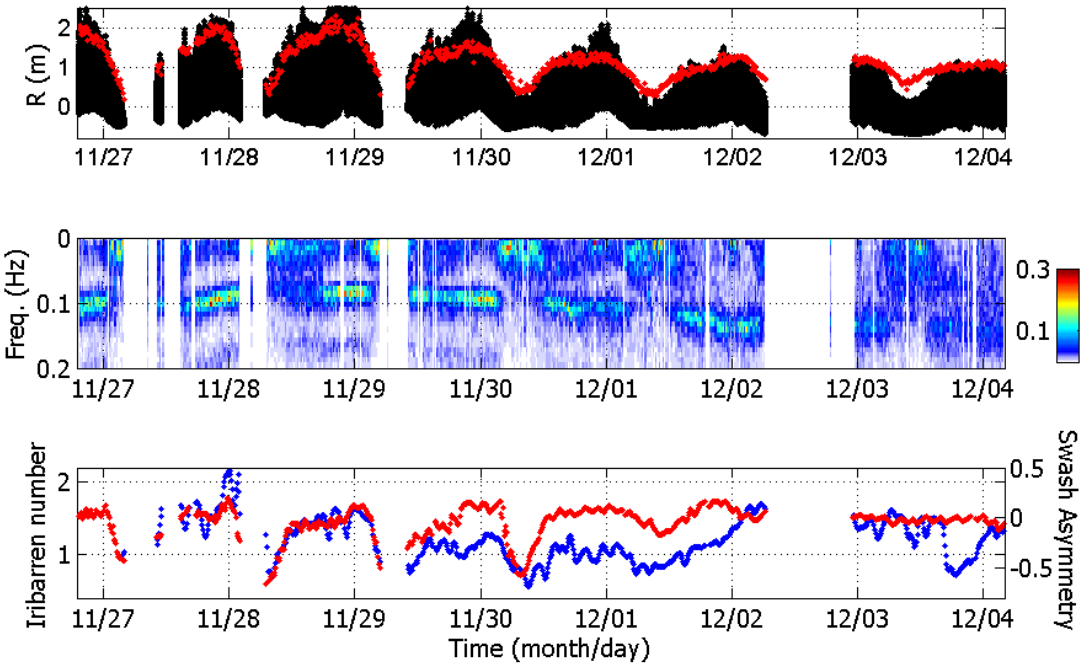

Figure 5. Time series of raw runup observation (black dots) and significant vertical runup (red dots - top panel); wave spectra measured at the breaking point (second panel); and Iribarren number (blue dots) with the overlap of swash asymmetry (red dots - bottom panel).

During low tide the lower water levels enhance wave breaking over the LTT, creating very dissipative conditions (lower Iribarren number). During this stage of the tide, the LTT acts as a low-pass filter to the swash zone (Waddell, 1973) dissipating much of the wave energy in the incident band (f between 0.3 and 0.05 Hz) leading to a dominance of infragravity motions (f between 0.05 and 0.03 Hz) as seen in Figure 5. At high tide, the LTT becomes less efficient at dissipating the energy of the incident waves. As such, waves reach the upper beach with higher steepness (larger wave heights than offshore but similar T_p), and

plunging breakers dominate the break point as indicated by the higher Irribarren numbers (Figure 5).The results suggest that tidal modulation of wave regimes, from dissipative to reflective, have an important impact on the swash asymmetry. Swash flows tend to be more asymmetrical (with negative A_s values) at low tide than at high tide (Figure 5).These tidal induced variations were more evident during spring tide and energetic wave conditions, while during neaps and milder wind waves A_s becomes less variable, with values generally close to zero.

3.4. *Swash zone morphodynamics*

The morphological feedback of the swash zone under such distinct hydrodynamic forcing was also investigated using the Lidar measurements. Time averaged (computed for consecutive segments of 10 minutes) beach profiles were used to compute the cumulative vertical changes for the entire duration of the experiment (Figure 6). Results show that during the energetic wave conditions observed in the initial days of this experiment erosion was observed in the upper part of the beach resulting in berm erosion (Figure 6). In the following days and under mild wave conditions it was observed that the beach developed significant recovery, with the formation of a new berm with a crest slightly lower than the previous existing one (Figure 6).

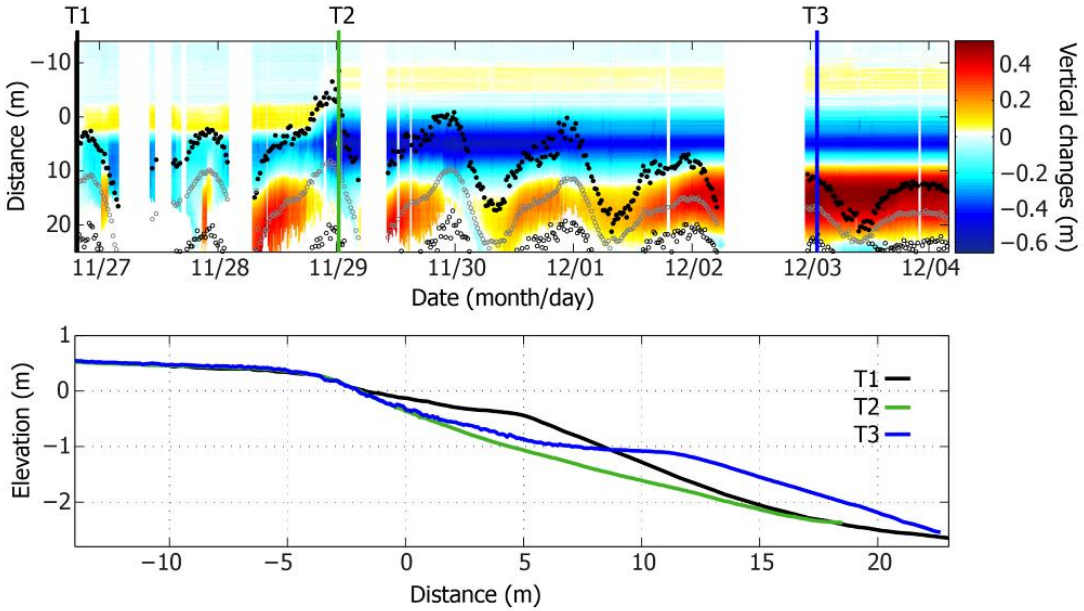

Figure 6. Morphological response of the beach during the Nha Trang experiment, with the cumulative vertical changes (top panel), and the indication of the maximum, minimum and average runup position (black and grey dots); the initial, middle and final beach profiles observed during this experiment are presented in the bottom panel.

The cumulative changes also provide interesting insights on the morphological response of the swash zone during the tide cycle, with asymmetrical morphological changes (accretion during rising and erosion during falling tide) occurring during the most energetic tides (Figure 6). Similar morphological response has been observed on mixed sand and gravel beaches with LTT (e.g., Kulkarni et al., 2004) or steep gravel beaches during energetic wave conditions (Almeida et al., 2015) however on sandy beaches with LTT this response was not observed before.

4. Discussion

Detailed field observations of swash zone hydrodynamics and morphodynamics were performed on a sandy beach with LTT using 2D LIDAR. The measurements obtained showed a good agreement with pressure transducers for water surface detection and conventional surveying approaches for beach profile measurements, confirming the applicability of the technology for remote sensing of various nearshore processes.

4.1 New insights on swash intra-tidal morphodynamics

Observations of morphological evolution in the swash zone, have shown a continuous and rapid adjustment of the beach to varying tide and wave conditions (Figure 6). In general, the morphological response of the swash zone during the experiment can be divided in two main episodes: (1) berm erosion; (2) neap-berm formation. In both cases the morphological response was a result of an increase in tidal range and reduction of offshore wave height. Larger high tides and bigger waves led to the overtopping of the initial berm and consequent erosion, while milder waves and neap tides led to the formation of a neap-berm (e.g., Hine, 1979; or Weir et al., 2006).

Intra-tidal LIDAR observations provided new insights on morphodynamic processes that have not be reported before on pure sandy beaches with LTT. Specifically the intra-tidal cycles of accretion and erosion during individual tide cycles between 27/11 and 01/12 (Figure 6). Based on the present dataset of field observations an interpretation of the mechanisms leading to the observed swash morphological changes is provided below.

Swash deposit formation

An accretion phase was identified between the low tide and the peak of the first high tide (Figure 6). This phase was characterized by a dissipative surf zone with spilling breakers dominating the entire surf zone, and infragravity and asymmetrical swash flows inundating the lower beach face (Figure 5). Such swash events characterized by fast inflows are expected to advect suspended sediments from the inner surf-zone into the uprush phase (Aagaard and Greenwood, 2008). Slower and long lasting backwash flows running over a gentler slope are expected to promote conditions for deposition (sediment have time to settle down before being taken by the backwash). This feedback between the hydrodynamics and morphology led to the development of a sandy deposit on the mi-lower swash zone (Figure 6). This accretion phase lasted until the first high tide peak and soon the tide rise again, the erosion phase is initiated.

Swash deposit erosion

The erosion of the deposit starts when the tide begins rising towards the second, larger magnitude high tide peak (Figure 6). An onshore migration of the surf and swash zone gradually modifies the hydrodynamic regimes with plunging breakers dissipating their energy on the steeper sections of the beach. At this point the deposit becomes gradually located under the breakpoint, thus directly under the highly turbulence generated by the plunging breakers which are believed to represent a key mechanism to entrain sediment from the break point into the water column (e.g., Brocchini and Baldock, 2008). Swash asymmetry during this period of time is reduced (swash horizontal excursions become symmetrical), indicating that the backwash is more capable of transporting sediment offshore (Figure 5). As the tide rises, the swash zone becomes steeper, inhibiting upslope transport and enhancing downslope transport and erosion of the deposit. This erosion phase ceases around the beginning of the ebb phase, when mean water level reach its maximum on the steeper section of the beach (Figure 6). Ebb phase is much faster than rising phase, and little modifications are observed in the morphology. Possible reasons for this result is the fact that the beach face is now in equilibrium with the wave conditions at all tide stages, or a result of the long relaxation time that these new morphological adjustments have face such fast rate of changes of the ebb.

Important to note that during mild wave conditions and neap tides the swash deposit was no longer dynamic and became a permanent morphological feature which led to the formation of a neap tide berm (Figure 6). It is very likely that at this point the swash morphology reached a new equilibrium with the

prevailing hydrodynamics, which is not affected by tide. Thus it is expected that the above described swash cyclic morphological behaviour will only occur when swash morphology is out of equilibrium with the tide and wave conditions.

5. Conclusions

The tide modulation of the surf and swash hydrodynamics and morphodynamics was investigated on a steep beach with low-tide terrace using a LIDAR. Observations performed with the LIDAR were found to have a good agreement with pressure-based estimations of water levels (r^2 0.85 and *rmse* 0.1 m) and RTK-GPS beach topographic measurements (r^2 0.99 and *rmse* 0.05 m). Daily observation showed that under energetic waves and large tide range upper beach was eroded (berm erosion) and a drop in the waves and tide range led to a rapid beach recover and the development of a new berm. New insights on the intra-tidal swash morphodynamics were measured by the LIDAR with individual tide cycles showing distinct phases of accretion and erosion. Accretion phase occurred between low tide and the first high tide peak, when surf zone was dominated by spilling breakers that advected sediment to the uprush, which in combination with slower backwash led to the development of a deposit in the lower-mid swash zone. Erosion phase started after the first high tide peak and lasted until the second high tide peak. This phase was characterised by plunging breakers breaking over steeper swash slopes, including over the swash deposit, in combination with less asymmetrical swash flows (similar uprush and backwash durations) leading to erosion of the previously formed deposit. Tide was found to play a crucial role in controlling surf and swash hydrodynamics which in combination with the important morphodynamic feedback lead to this intra-tidal swash cyclic morphological behaviour.

Acknowledgements

This research has received support from French grants through ANR (COASTVAR: ANR-14-ASTR-0019). The authors of this work would like to thank the support provided by all the participants present in this field experiment.

References

Aagaard, T., Greenwood, B., 2008.Infragravity wave contribution to surf zone sediment transport - The role of advection. *Marine Geology*, 251, pp. 1-14.

Almeida, L.P., Masselink, G., Russell, P., Davidson, M., 2015. Observations of gravel beach dynamics during high energy wave conditions using a laser scanner. *Geomorphology*, 228, pp. 15-27.

Battjes, J.A., 1974. Surf similarity. Proc. 14th Conference on Coastal Engineering, American Societyof Civil Engineers, pp. 466-480.

Blenkinsopp, C.E., Mole, M.A., Turner, I.L., Peirson, W.L., 2010. Measurements of the time-varying free-surface profile across the swash zone obtained using an industrial LIDAR. *Coastal Engineering*, 57, pp. 1059-1065.

Brodie, K.L., Raubenheimer, B., Elgar, S., Slocum, R.K., McNinch, J.E., 2015.Lidar and pressure measurements of inner-surfzone waves and setup. *Journal of atmospheric and ocean technology*, 32, pp.1945-1959.

Hine, A.C., 1979. Mechanisms of berm development and resulting beach growth along a barrier spit complex. *Sedimentology*, 26, pp. 333-351.

Hughes, M., Moseley, A. S., 2007.Hydrokinematic regions within the swash zone. *Continental Shelf Research* 27, pp. 2000–2013.

Kulkarni, C.D., Levoy, F., Montfort, O., Miles, J., 2004.Morphological variations of a mixed sediment beachface (Teignmouth, UK). *Continental Shelf Research*, 24, pp. 1203–1218.

Mau, L.D., 2014. Overview of Natural Geographical Conditions of Nha Trang Bay.Nha Trang: Institute of Oceanography.

Miles, J., Russell, P., 2004. Dynamics of a reflective beach with a low tide terrace. *Continental Shelf Research*, 24, pp. 1219-1247.

Puleo, J.A., Holland, K.T., 2001. Estimating swash zone friction coefficients on a sandy beach. *Coastal Engineering*, 43, pp. 25–40.

Raubenheimer, B., Guza, R.T., 1996. Observations and predictions of run-up. *Journal of Geophysical Research*, 101, pp. 25575–25587.

Ruggiero, P., R.A., Holman, and R.A. Beach, 2004.Wave run-up on a high-energy dissipative beach. *Journal of*

Geophysical Research, 109, pp. 1-12.

Thuan, D.H., Binh, L.T., Viet, N.T., Hanh, D.K., Almar, R., Marchesiello, P., 2016. Typhoon Impact and Recovery from Continuous Video Monitoring: a Case Study from Nha Trang Beach, Vietnam. *Journal of Coastal Research*, SI 75, pp. 263-267.

Weir, F.M., Hughes, M.G., Baldock, T.E., 2006.Beach face and berm morphodynamics fronting a coastal lagoon. *Geomorphology*, 82, pp. 331-346.